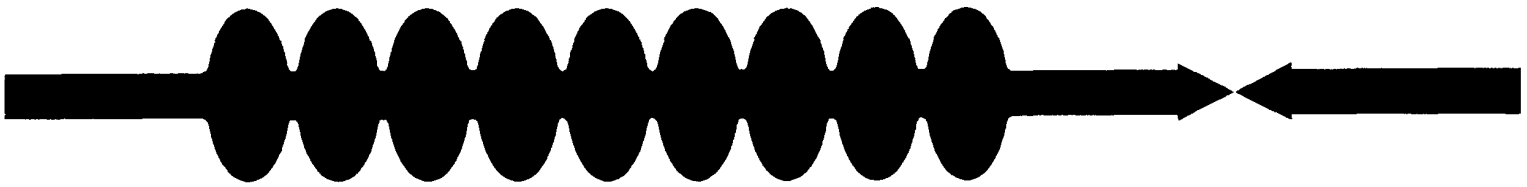

TESLA - COLLABORATION

The TESLA Beam Collimation System

R. Brinkmann, A. Drozhdin, D. Schulte, M. Seidel

DESY

December 1995, TESLA 95-25

TESLA Reports are available from:

Deutsches Elektronen-Synchrotron DESY
MHF-SL Group
Katrin Lando
Notkestraße 85
Postfach
22603 Hamburg
FRG

Phone: (0049/40) 8998 3339
Fax: (0049/40) 8994 4302
e-mail: LANDO@LANDO.DESY.DE

The TESLA Beam Collimation System

R.Brinkmann, A.Drozhdin, D.Schulte, M.Seidel

November 30, 1995

1 Introduction

At the TESLA beam parameters [1, 2] ($E = 250$ GeV, $N = 3.6 \cdot 10^{10}$ particles per bunch with 5650 bunches per second) the loss of a small fraction of the beam along the beam line effects strongly the background conditions in the detector and causes irradiation and heating of the Collider equipment.

The large aperture of the TESLA cavities are perceived to be a major advantage as it results in substantially reduced wake effects for both longitudinal and transverse wake fields. As the aperture of an L band cavity is equal to 70 mm, which is about ten times larger than in some of the higher frequency designs, relaxed linac alignment, injection jitter and vibration tolerances are possible. Coulomb scattering within the linac is negligible because of sufficiently low pressure in the superconducting linac compare to the conventional one. But since it may be true that even one particle hitting the final doublet can blind the detector, and large amplitude particles cause synchrotron radiation incident on the final doublet, a collimation system is necessary. It is necessary also for safety reasons, to protect the beam line and detector from destruction with a mis-steered beam.

The collimation system is intended to localize the beam loss in a specially equipped short part of the beam line to prevent particles loss in other parts of the Collider. The philosophy of the TESLA beam collimation system is to use large aperture quadrupoles and only collimate the beam at as large as possible amplitudes in order to minimize background produced by the collimators.

Particles tracking and beam loss simulations were done using a STRUCT code [3], where full scale beam line aperture simulations are performed. Calculation of the energy deposition in the collimation system components has been done with the GEANT code [4].

2 Collimation System Simulations

The layout of the TESLA beam collimation system is presented in Fig. 1. The requirements for beam collimation are determined by the condition that synchrotron radiation generated in the doublet before the IP has to pass freely through the aperture of the final quad on the opposite side. This means collimation of the so called "sine-like" trajectories (with respect to IP) at 12σ in X and 48σ in Y planes [2, 5]. The system consists of four "frame shape" titanium spoilers and four copper absorbers (we follow here concepts for mechanical collimation, originally developed at SLAC [6]). The spoilers are located at $8\sigma_x$ and $32\sigma_y$ transverse amplitudes, and at 2% momentum deviation in a region with large horizontal and vertical β-functions and maximum dispersion (Fig. 7). The spoilers are used to intercept particles with large momentum deviations and large amplitudes and to spoil a mis-steered beam or a beam with very large momentum deviation.

The first two spoilers are placed with a phase advance of π in between them to intercept "sine-like" trajectories. The second pair of spoilers is placed at $\pi/2$ phase advance downstream the first pair and intercepts "cosine-like" trajectories. Collimation of both phases becomes necessary because of the magnet lattice inserted between the collimation section and the Final Focus Section. Especially in the "big bend" section phase mixing can occur due to uncorrected chromaticity. Off-momentum trajectories which are purely sine-like at the IP can thus be (fully or partially) cosine-like at the entrance of the collimation section. Another consequence of phase mixing is that collimation at the two orthogonal phases must be tighter by a factor of $\sqrt{2}$ than the original requirement for sine-like trajectories at the IP.

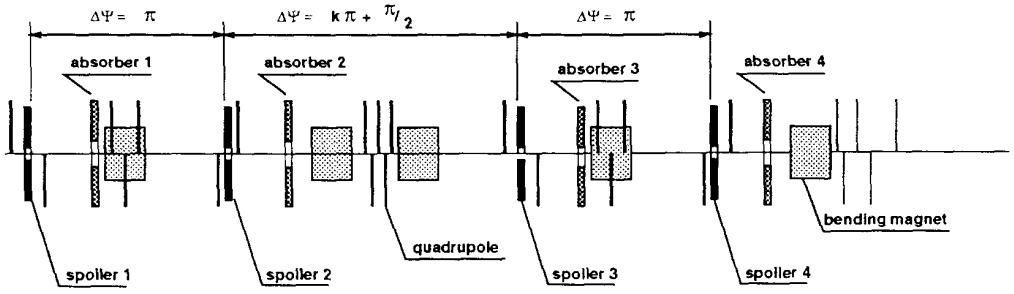

Figure 1: Scheme of the TESLA beam collimation system.

The absorbers are placed at $30\sigma_x$ and $100\sigma_y$ amplitudes. Due to the large amplitudes it becomes very unlikely that an unspoiled beam, which missed the spoilers, could hit them. Absorbers number 1,2,3 and 4 are used to protect magnets against irradiation with low energy electrons and secondary particles emitted from spoilers.

The jaw positions of the beam collimation system elements with respect to the beam axis are shown in Table 1.

element	SPOILERS				ABSORBERS			
number	1	2	3	4	1	2	3	4
X, mm	1.44	1.44	1.44	1.44	2.30	2.73	2.30	2.73
Y, mm	2.15	2.15	2.15	2.15	3.30	2.68	3.30	2.68
X, σ	8	8	8	8	30	30	30	30
Y, σ	32	32	32	32	100	100	100	100

Table 1: Jaws position of the beam collimation system elements with respect to the beam axis.

The beam loss in the absorbers and the amount of the spoiled beam which passes the collimation system are shown in Fig. 8 as a function of spoiler thickness.

The number of spoiled beam particles passed through the collimation system behind the fourth absorber is smaller than 10^{-3} for a spoiler thickness larger than 10 mm, and $4 \cdot 10^{-5}$ - for a thickness larger than 50 mm (Fig. 8). The beam size in the first absorber (absorber which intercepts most of particles) is equal to $\sigma_x = 4$ mm, $\sigma_y = 7$mm at 10 mm spoiler thickness, that is enough to absorb the beam safely. The advantage of the thin spoiler is a low energy deposition in the spoiler and therefore the possibility to accept a large number of bunches. However, the thick spoiler results in a two orders of magnitude higher efficiency of collimation system. Therefore we decided to use 70 mm thick spoilers which corresponds to two radiation lengths of Ti (see also section 5).

For the computer simulations of the background conditions in the IP, accelerator equipment irradiation and collimator heating the halo of the beam was represented by 10^6 particles with $1/x$ and $1/y$ density distributions for amplitudes of $A_x = (6-24)\sigma_x$ and $A_y = (24-100)\sigma_y$ and with momentum deviations of $\sigma(dP/P) = 1\%$. 0.01% of the beam are supposed to be outside the $(6 \times 24)\sigma_{xy}$ region in this simulations.

Particle loss distributions downstream the collimation region with and without collimation of the beam are shown in Fig. 9.

Beamstrahlung collimators and septum-magnet shadow [7] intercept large number of high amplitude particles. This decreases synchrotron radiation background in the detector. But interaction of these particles with collimators and shadow results in enormous fluxes of secondary particles on the detector components [8], causing radiation background.

If there is no collimation of the beam, about $1 \cdot 10^7$ and $2 \cdot 10^7$ electrons per second are lost in the seventh and eight bending magnets of the Final Focus System at magnet aperture diameter equal to $25mm$, $2.5 \cdot 10^8$ electrons - in the beamstrahlung dump number 1 downstream the last magnet at a distance of 98 m from the IP, $2.3 \cdot 10^5$ electrons - in the septum-magnet shadow at a distance

of 60 m from the IP, $5 \cdot 10^5$ electrons - in the doublet upstream the IP and $1 \cdot 10^6$ electrons per second - in the detector.

These losses are eliminated with collimation of the beam at $8\sigma_x$ X $32\sigma_y$. Even less tight collimation at $10\sigma_x$ X $40\sigma_y$ does not effect particle background in the detector (Fig. 9 bottom).

In Fig. 10 distributions of halo particles at the entrance of the second doublet of the Final Focus System for the beam without collimation and with collimation at $8\sigma_x$ X $32\sigma_y$, and at $10\sigma_x$ X $40\sigma_y$ are shown. The beam size without collimation is much larger compared to the beam whose synchrotron radiation passes freely through the aperture of the final quad on the opposite side ($A_x = 12\sigma_x = 4.3$ mm and $A_y = 48\sigma_y = 2.8$ mm) [2]. Even with collimation at $10\sigma_x$ X $40\sigma_y$, size of the beam is larger than necessary. This causes synchrotron radiation background in the detector.

The collimation system intercepts beam halo for the particles with a momentum deviation close to the equilibrium, but large momentum deviation particles spoil the picture. To improve that the second stage of collimation can be done in the high-β regions of the Final Focus System [9] about 200 m upstream the IP. These regions are situated $k\pi$ in phase advance from the last doublet, that is suitable for the "sine-like" trajectories collimation of the beam in horizontal and vertical planes. The distribution of halo particles for the two-stage collimation system is shown in Fig. 10.

The second stage of halo collimation gives us additional safety in suppressing background from large amplitude particles which may escape from the first stage or may be produced from gas-scattering between the collimation section and the Final Focus System. It also will help to keep the detector background at acceptable level even at a small deviations of the beam position in the first stage of collimation system.

This stage cleans the beam from large amplitude "sine-like" trajectories independently on the phase advance between the first stage and the IP. That gives the possibility for a future modifications of different parts of the beam delivery section without influence the collimation system efficiency.

The second stage of beam collimation permits to allow a reduction of the aperture of the beamstrahlung dump to R=4.3 mm since it reduces the amount of beam particles hitting the dump. The aperture reduction is necessary for synchrotron radiation interception (see below).

Particle loss distributions for the two-stage collimation system are shown in Fig. 11. The second stage spoilers are placed at $12\sigma_x$ and $48\sigma_y$ position to effect only large amplitude particles which cause synchrotron radiation in the last doublet before the IP. It intercepts 70 particles per bunch in our assumptions, what is about $5 \cdot 10^4$ times less than the first one (250 times smaller, for less tight first stage spoilers collimation at $10\sigma_x$ X $40\sigma_y$), but it is situated much closer to the IP. That is why the second stage can effect the muon background in the detector as well as the first one.

The layout of the second stage of the beam collimation system is presented in Fig. 2. The second stage is similar to the first one, but the first two spoilers are used for collimation of the beam in horizontal plane, and the second pair is used for vertical collimation. The jaw position of the beam collimation system elements with respect to the beam axis are shown in Table 2.

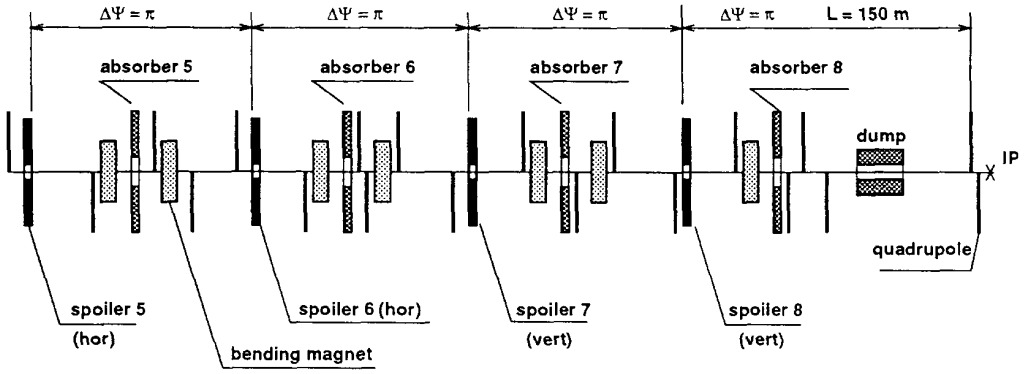

Figure 2: Second stage of the beam collimation system.

element	SPOILERS				ABSORBERS			
number	5	6	7	8	5	6	7	8
X, mm	1.90	1.90	2.00	2.00	2.50	2.50	2.50	2.50
Y, mm	2.00	2.00	1.80	1.80	2.50	2.50	2.50	2.50
X, σ	12	12	70	70	87	87	87	87
Y, σ	296	296	48	48	2500	2500	2500	2500

Table 2: Jaws position of the second stage beam collimation system elements with respect to the beam axis.

3 Synchrotron Radiation Background Simulations

The photon loss distributions emitted from the beam halo without collimation and with collimation of the beam with one- and two-stage systems are shown in Fig. 12 for collimation with the first stage spoilers at $8\sigma_x$ X $32\sigma_y$, and in Fig. 13 for collimation with the first stage at $10\sigma_x$ X $40\sigma_y$. The photon power losses in the 26 mm diameter vertex detector beam pipe [10, 11] amount to 0.00011 mW with two-stage collimation (0.0031 mW for less tight first stage collimation at $10\sigma_x$ X $40\sigma_y$), 0.00011 mW with one-stage collimation (0.0044 mW for less tight collimation at $10\sigma_x$ X $40\sigma_y$), and 33 mW without beam collimation.

Synchrotron radiation losses in the vertex detector emitted by the core of the beam in the last bending magnet as a function of beamstrahlung dump aperture radius are presented in Fig. 3 for two positions of beamstrahlung dump. Dump placed in a distance of 97 m from the IP eliminates synchrotron radiation loss in the detector at dump aperture radius smaller than 4.3 mm.

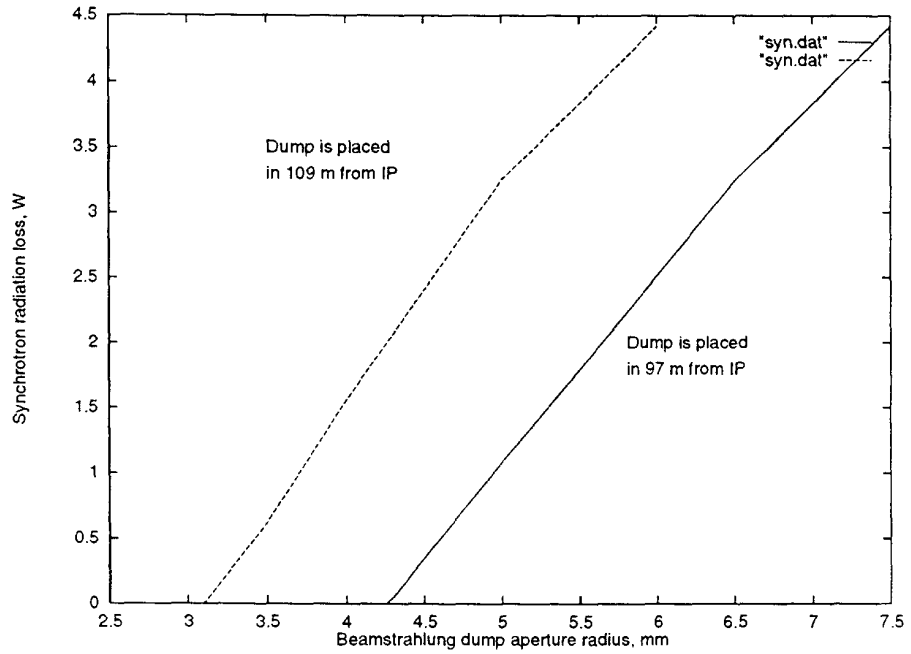

Figure 3: Synchrotron radiation losses in the vertex detector as a function of beamstrahlung dump aperture radius.

4 Secondary Particles Background Simulations

Simulation of secondary particles production was included in the elements with large rate of the beam loss. These elements are dump1, absorber number 8 and the septum-magnet shadow. These elements are assumed to be made from graphite here. The production of secondary particles in the energy range larger than 0.2 of the initial electron energy was taken into account in these simulations. Particle loss distributions for the system without beam collimation and with collimation with one- and two-stage systems are shown in Fig. 14

With collimation of the beam at $8\sigma_x$ and $32\sigma_y$, secondary particle fluxes in the vicinity of the IP are eliminated at all.

	$(dE/dx)_{min}$ [MeV/cm]	ρ [g/cm^3]	$c(T = 298\text{K})$ [J/gK]	λ [W/cmK]	X_0 [cm]
Ti	6.85	4.54	2.0	0.15	3.56
C	4.0	2.20	0.71	2...3	19.3

Table 3: Some properties of pyrolytic graphite and titanium.

5 Spoiler Design

The beam spoilers are intended to separate beam halo particles away from the beam so that these can be intercepted with thick absorbers at a downstream position in the beam line. This is achieved by two mechanisms - first the particles receive a relatively large kick angle in the spoiler due to multiple coulomb scattering which results in a blow up of the particle action and secondly the particles lose energy which brings them on dispersive trajectories. Especially the second mechanism provides a high efficiency for separating spoiled particles from the beam. For example the probability for a 250 GeV electron to travel through a 2 radiation length thick Ti spoiler without losing more than 10% of its energy is $5 \cdot 10^{-4}$.

The required properties of such a beam spoiler are partly in contradiction and a realistic design has to be a compromise with regard to several points which are described below.

5.1 Spoiler Heating in Case of an Accidental Beam Loss

Though the beam is enlarged at the spoiler position by optical magnification it still exhibits an enormous power density of $P_{tot}/2\pi\sigma_x\sigma_y \approx 140$ MW/mm^2. Of course there is no material which could withstand such a power density for a longer time. On the other hand the spoilers are close to the beam and one has to take into account the possibility that a mis-steered beam hits the spoiler head on. The spoiler should be able to accept at least a few bunches in such a case. During that time the beam loss can be detected and the remaining bunch train ($\approx$ 150 bunches if the damping ring extraction is switched off as fast as possible) can be dumped externally using an extraction kicker. Since the beam is small it might be even possible to sweep the remaining bunches over the spoiler. However, spoiler thickness and choice of material must be a compromise between the ability to strongly disrupt the energy of outcoming particles and on the other hand to withstand a number of head-on bunches.

We consider here two possibilities - a titanium spoiler and a graphite spoiler. Properties of both materials are given in table 3.

In Fig. 4 the peak energy deposition for one TESLA bunch with nominal dimensions is plotted as a function of depth (simulation with GEANT). Due to the large radiation length the graphite spoiler is much longer compared to

titanium. This leads to a larger transverse spread of the induced shower in graphite and results in a lower maximum energy deposition. In order to determine the instantaneous temperature jump due to the deposited energy one has to take into account the temperature dependence of the heat capacity:

$$\frac{dE}{dm} = \int_{T=T_0}^{T_0+\Delta T_{inst}} c(T)dT. \tag{1}$$

The instantaneous temperature jump ΔT_{inst} can be calculated by solving (1) numerically. Parameterizations for $c(T)$ can be found in [12], temperature curves for both materials are shown in Fig. 5.

The heating induces thermal stresses in the material which, if to high, will lead to cracks and damage the spoiler. The temperature limit can be estimated from the induced stresses:

$$\sigma_{UTS} > \frac{1}{2}\alpha E \Delta T_{inst}. \tag{2}$$

Here one should take into account that the material dependent parameters σ_{UTS} ultimate tensile strength, α linear expansion coefficient and E elastic modulus are also functions of temperature. From (2) we estimate limits of $\approx$ 1000 °C for Ti and 2650 °C for pyrolytic graphite. From the temperature curves in Fig. 5 it can be concluded that both materials are suited for a beam spoiler and can withstand a sufficient number of bunches. However, a two radiation length thick pyrolytic graphite spoiler can accept nearly 50 bunches on the same spot whereas the equivalent titanium spoiler stands only 6 bunches. Therefore a graphite spoiler would promise a higher inherent safety in case of accidental beam losses. Another advantageous property of graphite is its large thermal conductivity λ which becomes important if relatively large steady beam losses on the spoilers have to be handled. Such a situation is imaginable for instance during set-up and tuning of the machine. A disadvantage of graphite is certainly the larger length of the spoiler which results in a higher probability for edge scattering and reduces the collimation efficiency.

5.2 Emittance Dilution by Wakefields

Ultrarelativistic particles moving in a perfectly conducting pipe experience no transverse kick since the forces caused by the electric and magnetic field cancel exactly. However, at discontinuities as the entrance or the exit of a beam spoiler this cancelation is distorted and particles in a off-axis bunch will experience an effective kick due to the induced fields. The so called geometric wake field kick varies along the longitudinal direction of the bunch and can be estimated for rectangular spoilers by [13]:

$$\Delta y'(z) = \theta_1 \exp\left(-\frac{z^2}{2\sigma_z^2}\right); \quad \theta_1 = \frac{\pi^2 r_e N_B}{2\sqrt{2\pi}\gamma\sigma_z}\frac{\langle\Delta y\rangle}{g}, \tag{3}$$

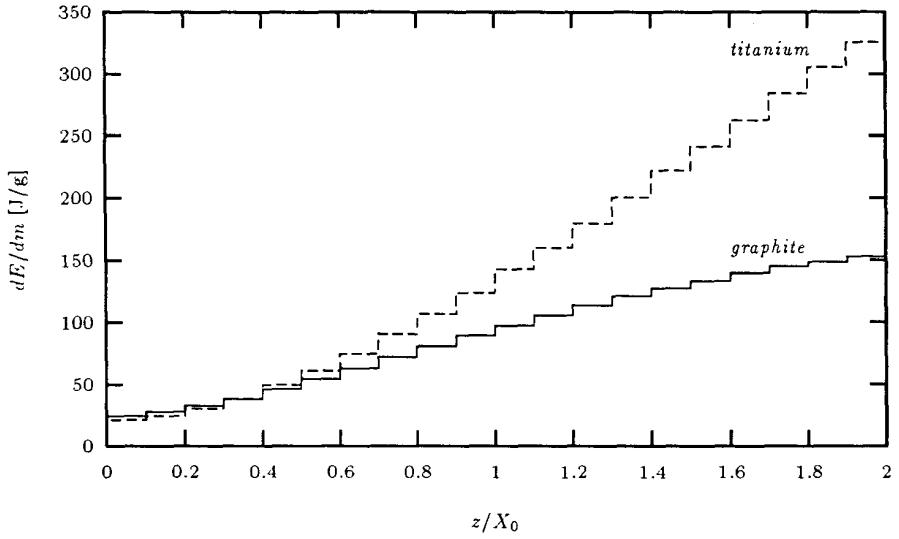

Figure 4: Energy deposition of one TESLA bunch in graphite and titanium on the beam axis as a function of depth.

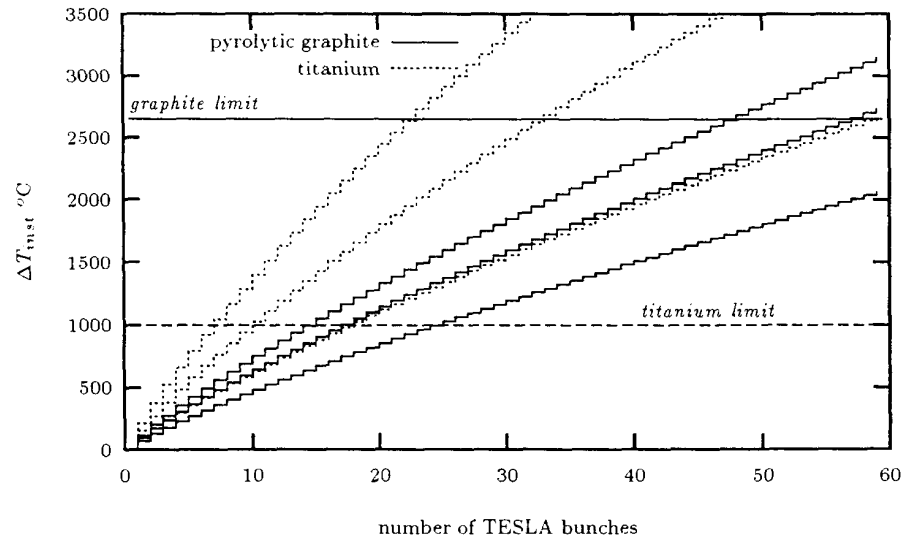

Figure 5: Instantaneous temperature rise in graphite and titanium as a function of the number of TESLA bunches hitting the spoiler. The three curves for each material correspond to depths of 1.0, 1.5, 2.0 radiation lengths.

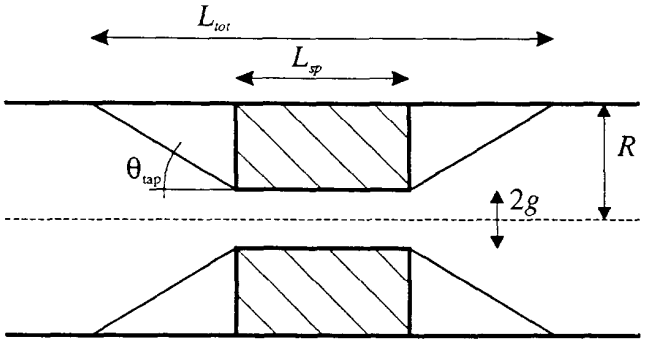

Figure 6: Sketch of the tapered spoiler.

where $r_e = 2.8 \cdot 10^{-15}$ m the classical electron radius, $\sigma_z = 0.7$ mm the rms bunch length, $N_B = 3.6 \cdot 10^{10}$ the bunch population, $\langle \Delta y \rangle$ the transverse bunch offset and g the half gap between the spoilers.

Since the strength of the kick varies along the bunch it dilutes the beam emittance. We assume that the mean kick can be corrected with steering elements and demand a luminosity reduction of less than 2 %:

$$\frac{\Delta L}{L} = \frac{1}{2}\frac{\Delta \varepsilon}{\varepsilon} = \frac{1}{2}\frac{\Delta y'^2_{rms}}{\sigma'^2} \leq 0.02, \text{ or } \quad \Delta y'_{rms} \leq \frac{1}{5}\sigma'.$$

The rms-wakefield kick $\Delta y'_{rms}$ is obtained by averaging of $\Delta y'$ and $\Delta y'^2$ over the longitudinal charge distribution (which is assumed here to be Gaussian):

$$\Delta y'_{rms} = \left(\langle \Delta y'^2 \rangle - \langle \Delta y' \rangle^2\right)^{\frac{1}{2}} = \left(\frac{2-\sqrt{3}}{2\sqrt{3}}\right)^{\frac{1}{2}} \theta_1 = 0.278 \cdot \theta_1.$$

In order to reduce the geometric wakefield the spoiler can be tapered as shown in Fig. 6. For taper angles $\theta_{tap} \ll 1$ the reduction factor is a linear function of θ_{tap} [14]:

$$k_1 = \frac{6\theta_{tap}}{\pi} \approx \frac{12(R-g)}{\pi(L_{tot} - L_{sp})}. \tag{4}$$

Of course the beam spoilers are not perfect conductors and for narrow gaps the resistive losses act back on the bunch. The so called resistive wall wakefield kick can be estimated by [15]:

$$\Delta y'(z) = \theta_2 \frac{1}{\sqrt{2\pi}} \int_{s=0}^{\infty} \frac{ds}{\sqrt{s}} \exp\left(-\frac{(z-s)^2}{2}\right); \quad \theta_2 = \frac{\pi^2 r_e N_B L_{sp}}{2\gamma} \sqrt{\frac{\lambda_{sp}}{\pi \sigma_z}} \frac{\langle \Delta y \rangle}{g^3}, \tag{5}$$

where L_{sp} is the length of the spoiler and λ_{sp} is a characteristic length calculated[1]

[1]Note that we use MKSA units throughout this paper. In CGS units the conductivity is smaller by a factor $4\pi\epsilon_0$ and the kick formulas are different as well.

from the conductivity σ_{sp} of the spoiler material:

$$\lambda = \frac{1}{c\mu_0\sigma_{sp}}.$$

Here the rms-kick is given by [6]

$$\Delta y'_{rms} = \left(\frac{K(\sqrt{3}/2)}{2\sqrt{\pi}} - \frac{\Gamma^2(1/4)}{8\pi}\right)^{\frac{1}{2}} \cdot \theta_2 = 0.292 \cdot \theta_2.$$

Tapering increases the length of the spoiler and therefore the resistive wall kick. The increase can be estimated by replacing the factor $\sqrt{\lambda_{sp}}L_{sp}/g^3$ in (5) by an integral over the total length:

$$\frac{\sqrt{\lambda_{sp}}L_{sp}}{g^3} \approx \int_{l=0}^{L_{tot}} \frac{\sqrt{\lambda(l)}}{g^3(l)}\, dl.$$

Thereby we obtain an enlargement factor for the rms-resistive wall wakefield kick of the tapered spoiler of (see geometry in Fig. 6)

$$k_2 = 1 + \frac{1}{2}\sqrt{\frac{\lambda_{tap}}{\lambda_{sp}}}\left(\frac{L_{tot}}{L_{sp}} - 1\right)\left(1 + \frac{g}{R}\right)\frac{g}{R}. \qquad (6)$$

Here λ_{tap} is the characteristic length of the taper material which could be a thin copper foil for instance. Note that the heating of the taper material is not critical since the beam spot is enlarged by $1/\theta_{tap}$.

As long as the resistive wall wakefield kick is smaller than the geometric wakefield kick, tapering of the spoiler is helpful. The optimum total length of the tapered spoiler L_{tot} is achieved when both kicks have equal strength:

$$0.278 \cdot k_1(L_{tot}) \cdot \theta_1 = 0.292 \cdot k_2(L_{tot}) \cdot \theta_2.$$

Now we can apply these formulas to the TESLA parameters. We consider three possible layouts for the spoiler - a spoiler made of pyrolytic graphite, the graphite spoiler with copper coating and a spoiler made of titanium. For all kinds of spoilers we assume a thickness of 2 radiation lengths and a radius of the beam-pipe of $R = 12.5$ mm. TESLA parameters relevant for the beam spoilers are given in table 4, material parameters in table 5 and results for the different layouts in table 6. It turns out that the graphite spoiler, even untapered, misses the goal of $\Delta y'_{rms} \leq \sigma'/5$ already due to the resistive wall effect (see table 6). So tapering will not improve the situation in that case. However, the Ti spoiler is uncritical if one applies some tapering. If coating of the inner surface of the graphite spoiler with a thin layer of copper or another material with high electrical conductivity is possible, also such a design could be used.

The conclusion from these considerations is that mechanical collimation of the TESLA beam at amplitudes of $8\sigma_x$ and $32\sigma_y$ can be realized with a tapered Ti spoiler. A graphite spoiler would be advantageous in view of its thermal properties, however, it remains to find a method to reduce the surface resistance.

	$\gamma\varepsilon$ [mm mrad]	β [m]	σ [μm]	σ' [nrad]	g [mm]	g/σ
X:	14	868	158	181	1.3	8
Y:	0.25	6797	59	8.7	1.9	32

Table 4: Some beam related parameters at the spoiler locations.

	$C_\perp$	$C_\parallel$	Ti	Cu	Au
λ [m]	$2.65 \cdot 10^{-6}$	$1.06 \cdot 10^{-8}$	$1.47 \cdot 10^{-9}$	$4.5 \cdot 10^{-11}$	$6.1 \cdot 10^{-11}$

Table 5: Characteristic length of several materials. Note the anisotropic properties of pyrolytic graphite. We assume that the material is aligned along the beam in the direction of the higher conductivity.

	geometric		resistive wall		opt. tapered		opt. len. [m]	
	$\frac{\sigma'_x}{\Delta x'_{rms}}$	$\frac{\sigma'_y}{\Delta y'_{rms}}$	$\frac{\sigma'_x}{\Delta x'_{rms}}$	$\frac{\sigma'_y}{\Delta y'_{rms}}$	$\frac{\sigma'_x}{\Delta x'_{rms}}$	$\frac{\sigma'_y}{\Delta y'_{rms}}$	L^x_{tot}	L^y_{tot}
C	9.0	1.7	9.4	4.0	-	-	-	-
C,Cu	9.0	1.7	142.1	60.7	130.2	48.1	1.0	1.5
Ti	9.0	1.7	132.8	56.7	122.8	45.9	0.66	1.2

Table 6: Wakefield kicks for different spoiler materials and taperings for a beam offset of 1 σ. The table contains the geometric and resistive wall kicks for the untapered spoiler and the geometric kicks for an optimal tapered spoiler. Given is always the value of $\sigma'/\Delta y'_{rms}$ which should be larger than 5 for a luminosity reduction of less than 2%. Furthermore the total length for an optimal tapered spoiler is given.

6 Conclusions

1) Only using thick spoilers (larger than two radiation lengths) is possible to get high efficiency of the beam halo collimation in TESLA.

2) One-stage beam collimation system which intercepts sine- and cosine-like trajectories at $8\sigma_x$ and $32\sigma_y$ permits to eliminate particle loss in the detector and to decrease the synchrotron radiation loss emitted from halo in the last Final Focus System doublet $3.0 \cdot 10^5$ times.

3) The second stage of halo sine-like trajectories collimation placed in the high-β regions of the Final Focus System permits to clean the beam from large amplitude particles independently on phase advance between the first stage and the IP. This gives the possibility for a future modifications of different parts of the beam delivery section without influence the collimation system efficiency.

4) The concept of mechanical collimation with tapered titanium spoilers is applicable for TESLA. Emittance dilution due to wakefields is negligible and the requirement for spoiler protection to trigger the safety dump kicker after no more than six bunches (or $4.2\mu s$) is realistic.

References

[1] H.T.Edwards. TESLA Parameters Update a Progress Report on the TESLA Collider Design. March, Particles Accelerators,1994,Vol.XX.

[2] R.Brinkmann. Status of the Design for the TESLA Linear Collider. Particle Accelerator Conference, Dallas 1995, DESY-TESLA 95-11. p.33.

[3] I.Baishev, A.Drozhdin, N.Mokhov. STRUCT Program User's Reference Manuel. SSC-MAN-0034, February 1994.

[4] GEANT Program User's Reference Manuel.....

[5] R.Brinkmann. Final Doublet Apertures, Collimation Requirements. 15/09/93.

[6] N.Merminga, J.Irwin, R.Helm, R.D.Ruth, Collimation Systems for a TEV Linear Collider, SLAC Pub. 5165 Rev. (1994)

[7] A.Drozhdin, Extraction of the Spent Beam into the TESLA Beam Capture Section, DESY Print, December 1994, TESLA 94-29.

[8] M.Sachwitz, H.J.Schreiber. Muon Background. TESLA meeting, Frascati, November 8-10, 1994.

[9] O.Napoly, E.Klein, J.M.Rifflet, TESLA Final Focus System with Superconducting Magnets in the Interaction Region: Optics, Tolerances and Magnet Design, DESY Print, December 1994, TESLA 94-31.

[10] D.Schulte. Summary of TESLA 500 Working Groups. TESLA test facility meeting, Orsay, March 8-10, 1994. D.Schulte. Schematic Layout of the Interaction Region. TESLA test facility meeting, Orsay, March 8-10, 1994.

[11] Daniel Schulte. Background in the Interaction Region. TESLA meeting, Frascati, November 8-10, 1994.

[12] Handbook of Chemistry and Physics, Chemical Rubber Publishing Company (1976)

[13] K.L.F. Bane, P.L. Morton, Deflection by the Image Current and Charges of a Beam Scraper, SLAC Pub. 3983 (1986)

[14] Kaoru Yokoya, Impedance of Slowly Tapered Structures, CERN SL/90-88 (1988)

[15] A.Chao, Physics of Collective Beam Instabilities in High Energy Accelerators, J.Wiley & Sons, New York (1993)

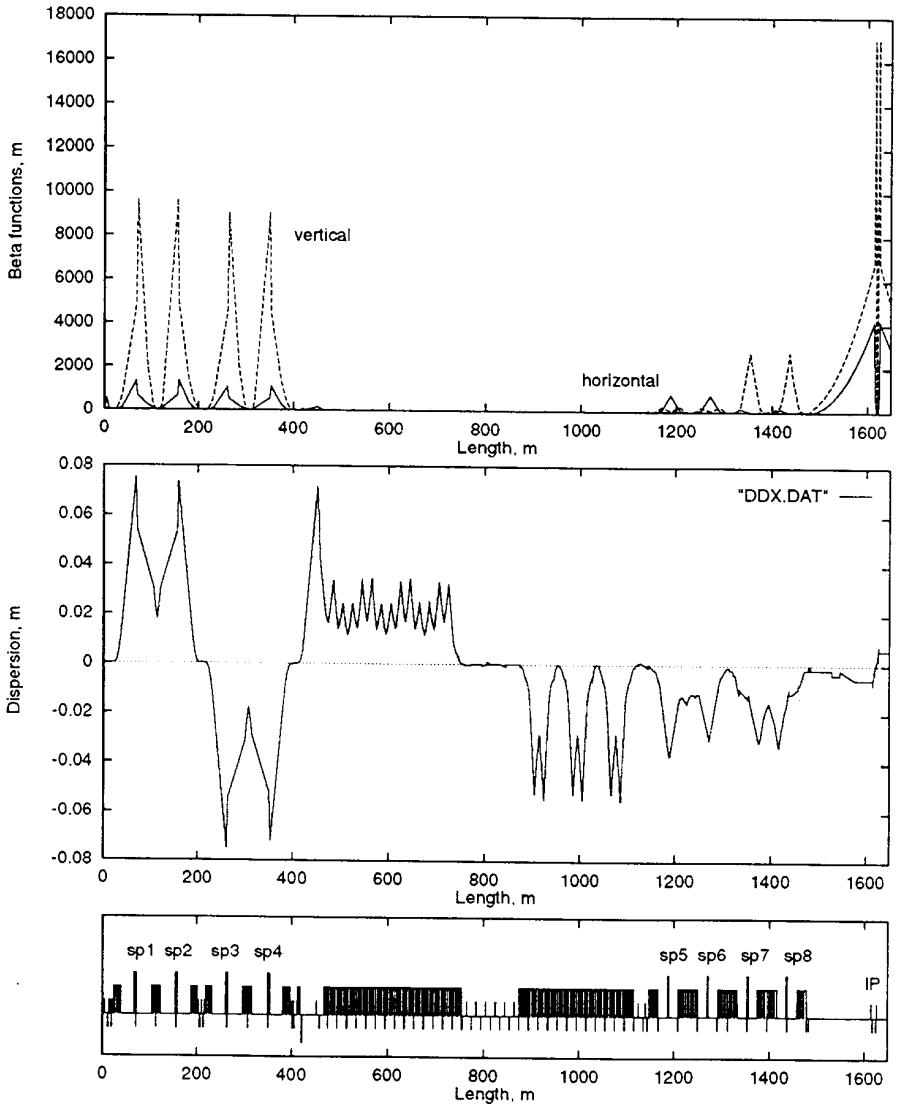

Figure 7: Horizontal β-function (solid line) and vertical β-function (dashed line) in the collimation region (top). Horizontal dispersion function (bottom).

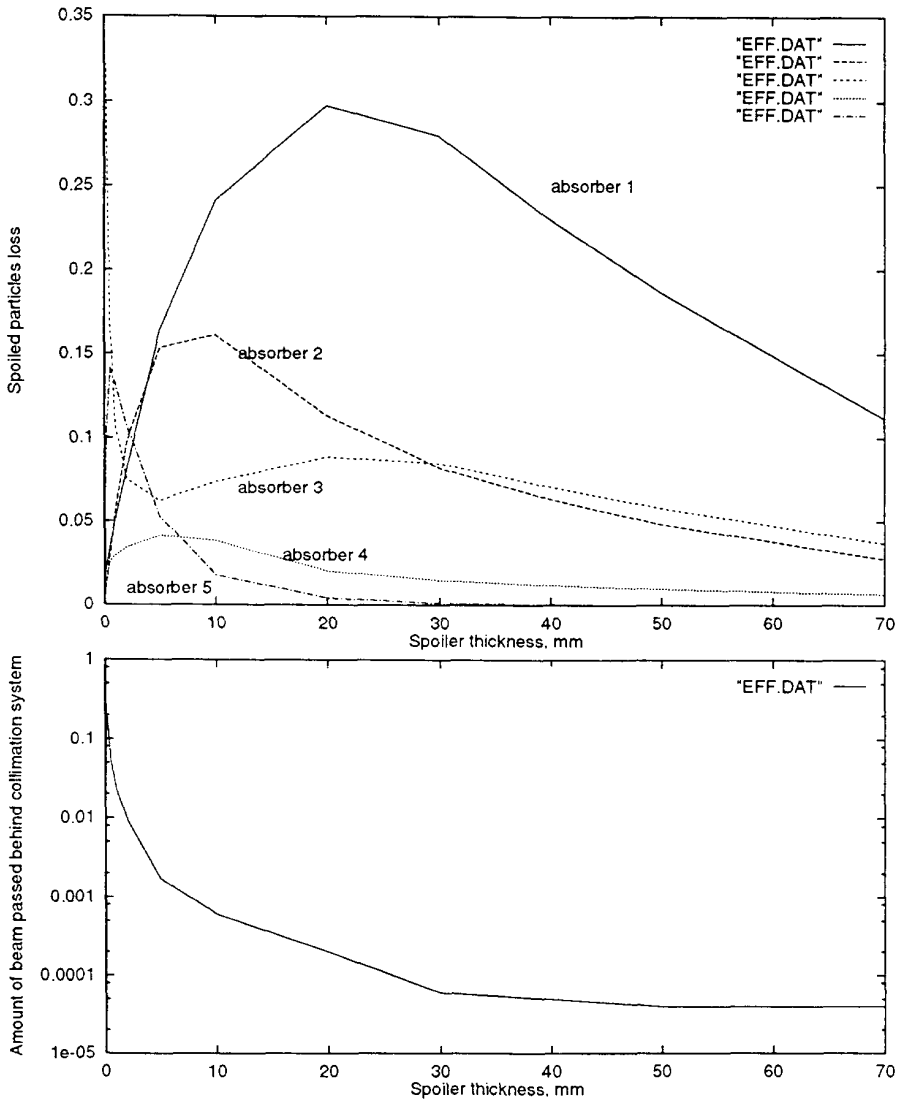

Figure 8: Beam loss in the absorbers and amount of the spoiled beam passed behind the fourth absorber.

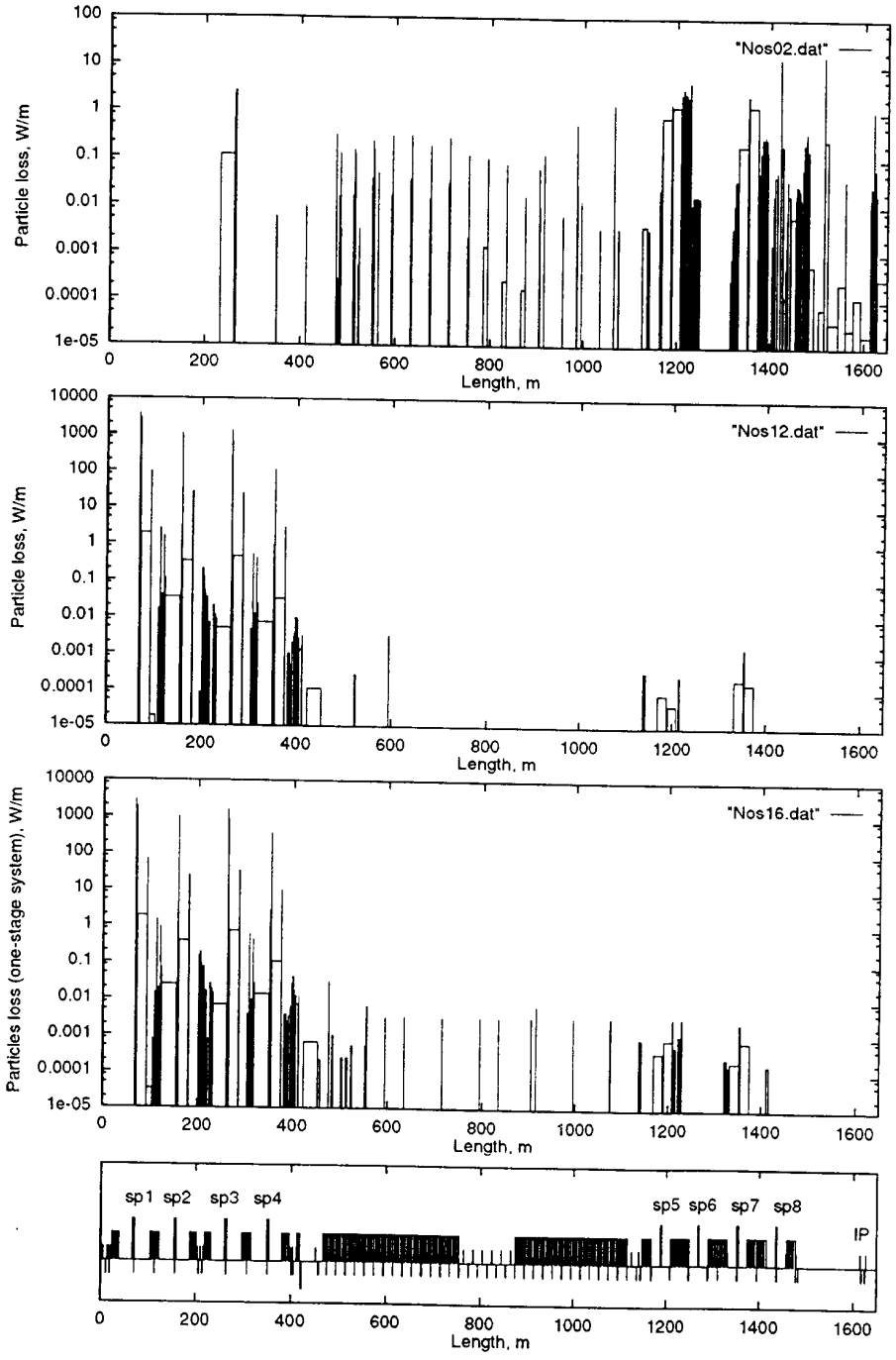

Figure 9: Particle loss distributions without collimation (top), with collimation of the beam with one-stage system at $8\sigma_x$ X $32\sigma_y$ (middle), and at $10\sigma_x$ X $40\sigma_y$ (bottom).

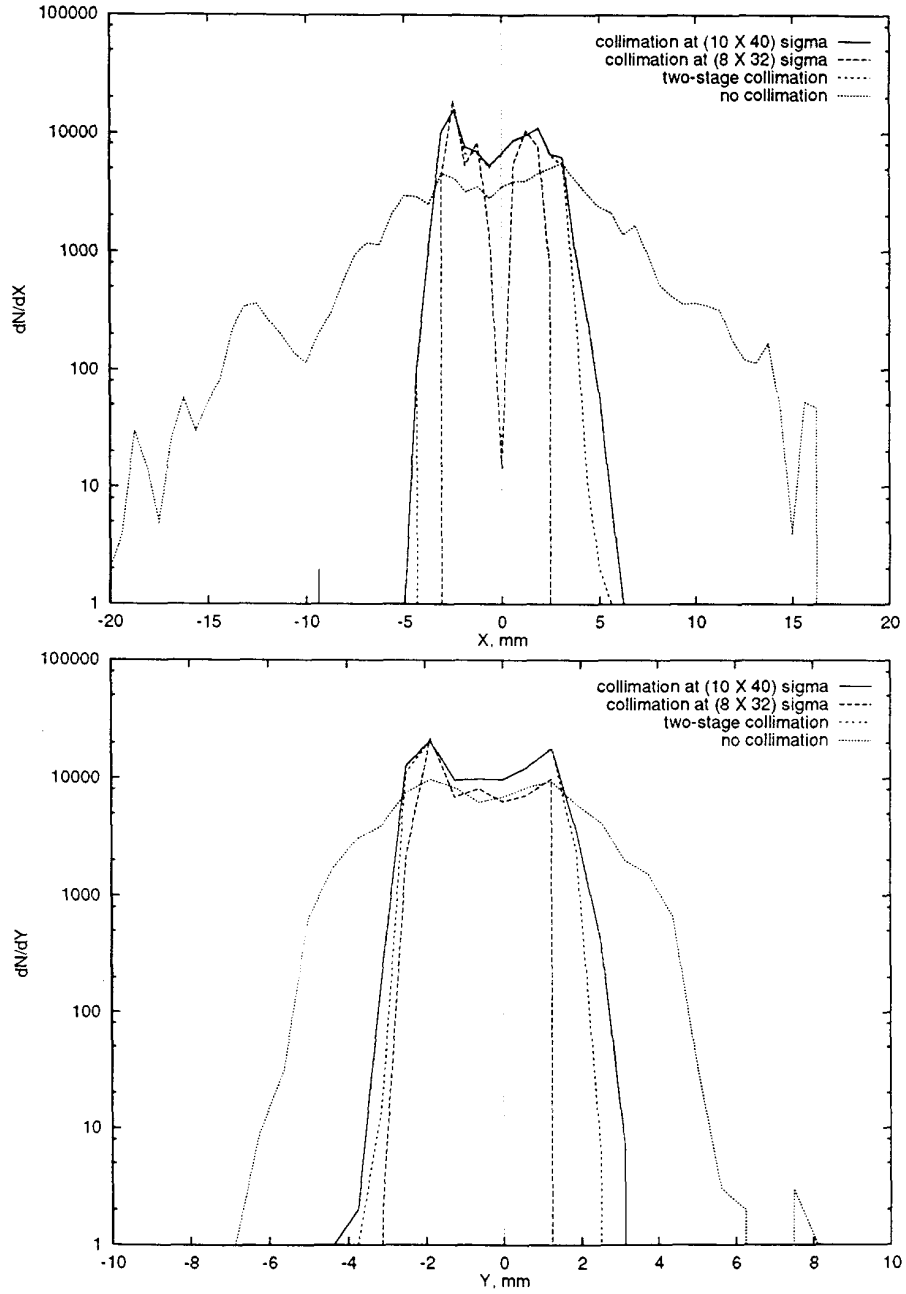

Figure 10: Halo particle distributions at the entrance of the second doublet of the Final Focus System for the beam without collimation, with collimation of halo with one-stage system (at $8\sigma_x$ X $32\sigma_y$ and at $10\sigma_x$ X $40\sigma_y$), and with two-stage collimation system.

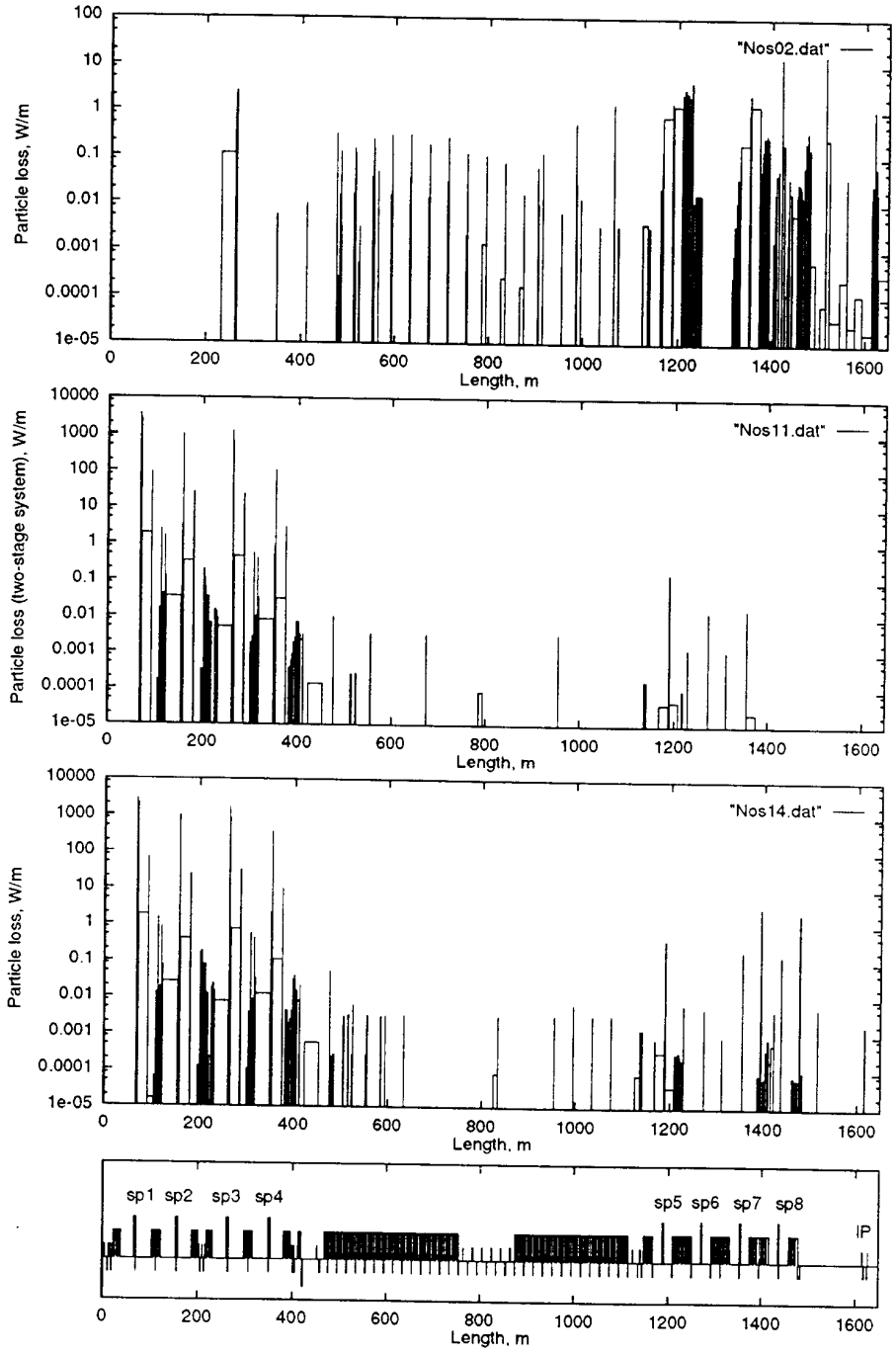

Figure 11: Particle loss distributions for the beam without collimation (top), and for collimation of the beam with two-stage system at collimation with the first stage at $8\sigma_x$ X $32\sigma_y$ (middle), and at $10\sigma_x$ X $40\sigma_y$ (bottom).

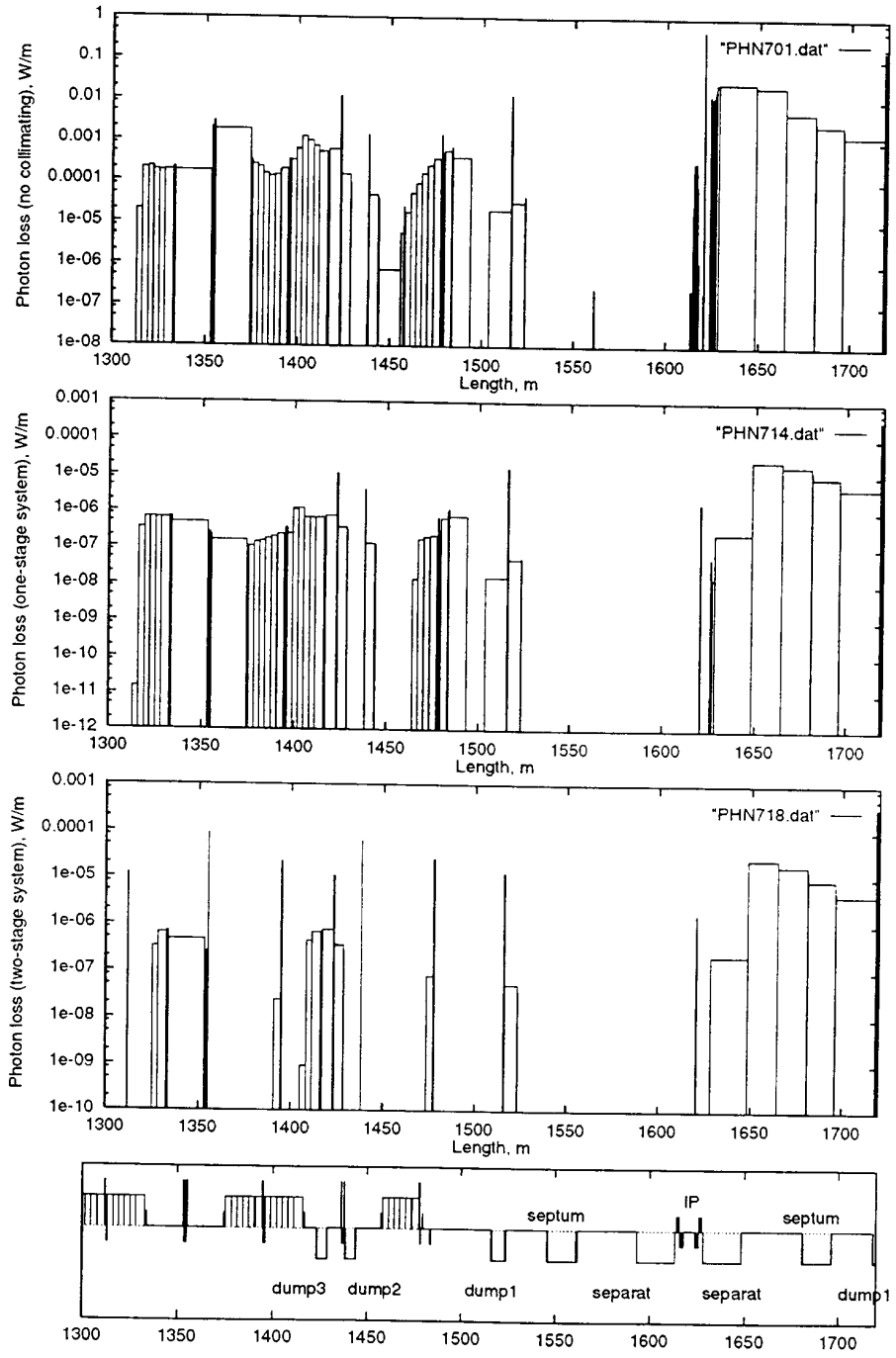

Figure 12: Photon loss distributions emitted from the beam halo without collimation, and with collimation of the beam with one- and two-stage systems for collimation with the first stage at $8\sigma_x$ X $32\sigma_y$.

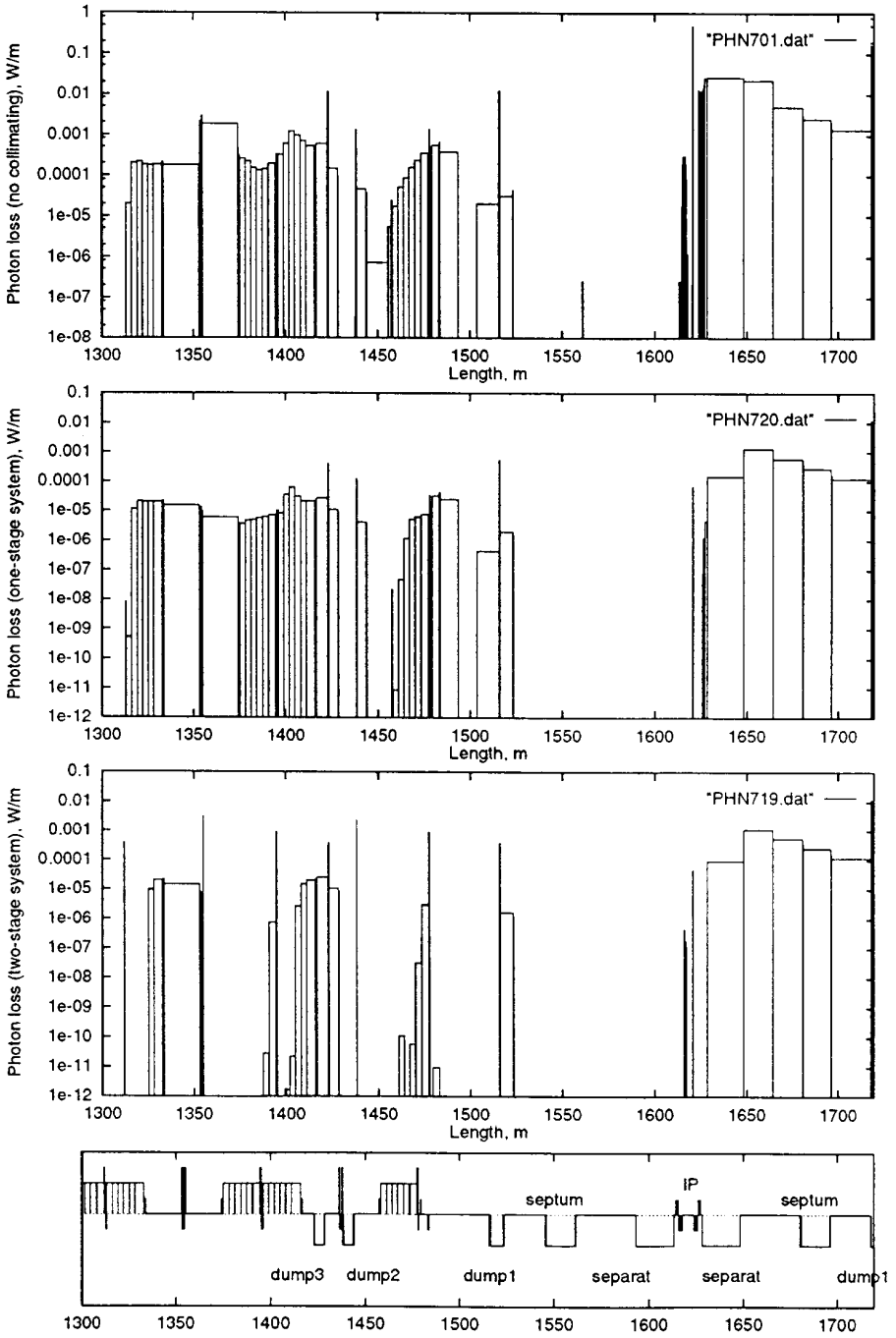

Figure 13: Photon loss distributions emitted from the beam halo without collimation, and with collimation of the beam with one- and two-stage systems for collimation with the first stage at $10\sigma_x$ X $40\sigma_y$.

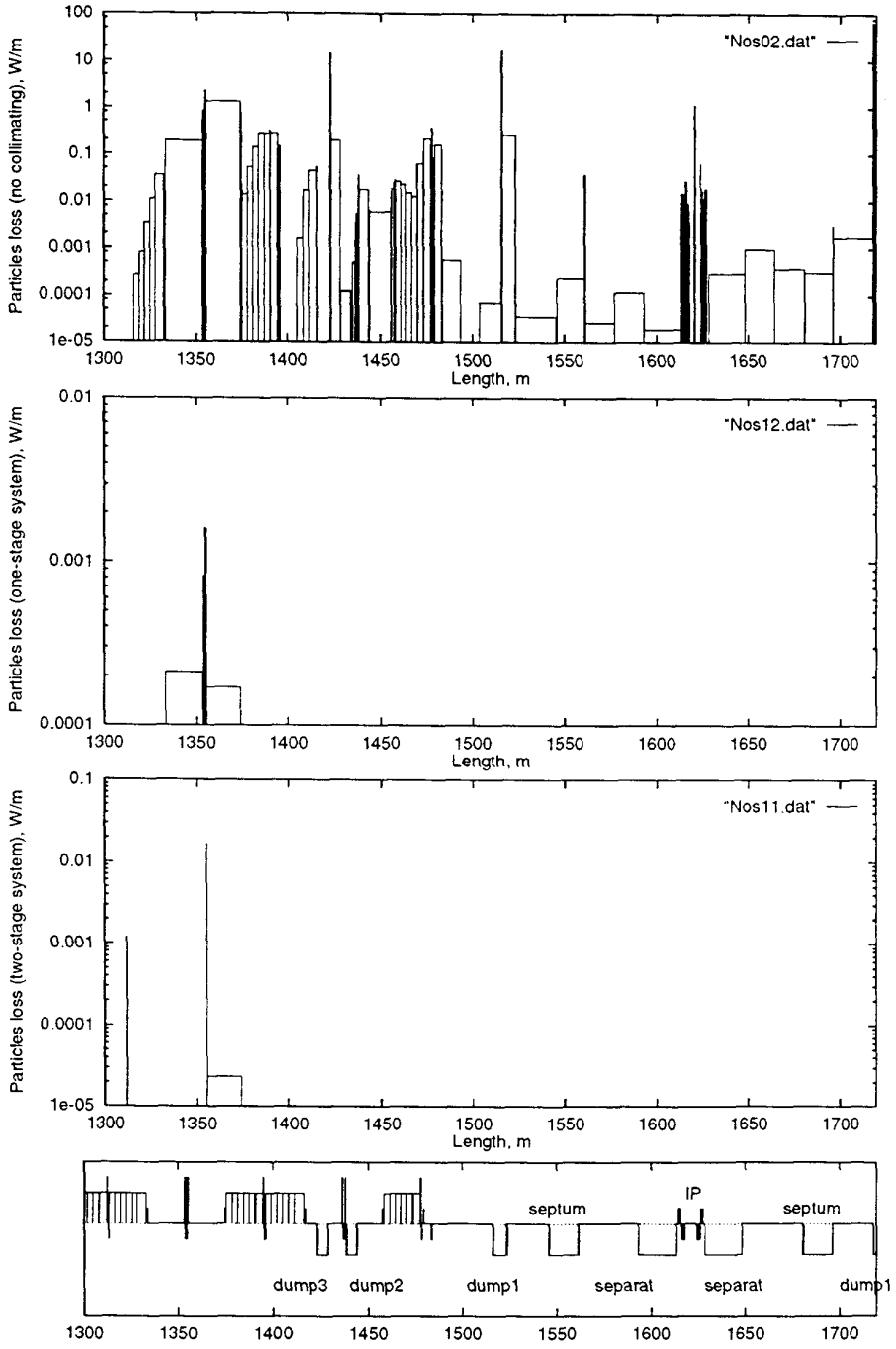

Figure 14: Primary and secondary particle loss distributions in the IP region without beam collimation (top), and with collimation of the beam with one- and two-stage (bottom) systems for collimation with the first stage at $8\sigma_x$ X $32\sigma_y$.